

Examination of the Relationship Between Spectral Type and Stellar Rotational Velocity in ~50,000 Single Stars

Boran Mert¹, Usta Ahmet¹ and Kayhan Cenk^{1,2,*}

¹Department of Astronomy and Space Sciences, Science Faculty, Erciyes University, 38030 Melikgazi, Kayseri, Türkiye²Scientific Research Projects Coordination Unit, Kayseri University, 38280 Talas, Kayseri, Türkiye

*Corresponding author. E-mail: cenkayhan@erciyes.edu.tr

MS received XX April 2024; accepted XX November 2024

Abstract. In this study, we present the results of the relationship between spectral type (ST) and the projected stellar rotational velocity ($v_{\text{sin}i}$), utilising a sample of approximately 50,000 single stars across a range of evolutionary stages. The STs of the stars included in this study span a broad range, from O0 to M9. We examine the stars in our data set, which has been divided into two groups according to ST and luminosity class (LC). The groups were conducted an investigation into the relationship between the mean $v_{\text{sin}i}$ ($\langle v_{\text{sin}i} \rangle$) and STs, as well as the dependence of $\langle v_{\text{sin}i} \rangle$ on STs and LCs. The rationale for investigating the two subgroups separately is to take into account for the evolutionary status of the stars and ascertain the impact on stellar rotation. The results demonstrate a notable decline in $\langle v_{\text{sin}i} \rangle$ as the spectral type progresses from early to late types. In particular, we found a significant decrease in $\langle v_{\text{sin}i} \rangle$ values, amounting to approximately 100 km/s, between hot stars (STs O0 to F2) and cool stars (STs F2 to M9). Moreover, a reduction in $\langle v_{\text{sin}i} \rangle$ is discernible as stars evolve, with this trend being most pronounced in evolutionary stages beyond the subgiant phase.

Keywords. Stellar Rotation—Spectral Type—Luminosity Class

1. Introduction

All stars are born within molecular clouds, evolve over time, and ultimately reach the end of their evolution. The parameters that determine the manner in which this radiant life will unfold represent a complex puzzle. It is essential to gain an understanding of each piece and to place it correctly. Among these parameters, stellar rotation is a factor that exerts a significant influence on the overall structure of the star, from the stellar core to the stellar surface. The most significant study on stellar rotation was conducted by von Zeipel (1924), which demonstrated that stellar rotation is a crucial parameter in stellar evolution. One of the most readily apparent consequences of stellar rotation is the alternation of stellar shape, manifested as a departure from spherical symmetry (McAlister *et al.*, 2005; Che *et al.*, 2011). Consequently, based on certain observations, there is the potential for a variation of up to 50% between the radius of the polar and equatorial regions (Maeder, 2009; Abdul-Masih, 2023). Such alternations in radius result in a modified effective temperature profile and ionisation equilibrium of the star (von Zeipel, 1924; Maeder, 2009). An additional consequence of stellar rotation is the alternation of the chemical com-

position of the star. Differential rotation disrupts the equilibrium of the stellar core and layers, prompting the mixing of matter within the core and radiative envelope (Jermyn *et al.*, 2018; Costa *et al.*, 2019). Some studies have demonstrated that rotational mixing can enhance the supply of hydrogen within the stellar core, thereby prolonging the lifespan of the main-sequence (MS) phase by approximately 30% (Meynet & Maeder, 2000). In the initial stages (first few million years) of stellar evolution, as evidenced by multiple studies (e.g. Rebull *et al.* (2006); Cieza & Baliber (2007); Gallet & Bouvier (2013)), stars with accretion discs tend to exhibit slower rotation rates than those without discs. The primary rationale for this phenomenon can be attributed to the disc-locking hypothesis, which posits that the star remains attached to the disc, thereby maintaining a constant projected stellar rotational velocity ($v_{\text{sin}i}$). It has been demonstrated by various studies (e. g. Koenigl (1991); Collier Cameron & Campbell (1993); Armitage & Clarke (1996)), that the interaction between a star and a stellar disc with a magnetic field can regulate $v_{\text{sin}i}$ of the central star, resulting in the star becoming tidally locked (Barnes *et al.*, 2001). This will result in a reduction in $v_{\text{sin}i}$ of the star. However, when the star loses its disc, it undergoes a period of rapid rotation

as a consequence of the anticipated radius contraction along the Hayashi track (Gallet & Bouvier, 2013). As evidenced by prior studies in the literature, this phenomenon can be attributed to the inability of the star to sustain its angular momentum from the zero-age MS (ZAMS) to MS.

The magnetic effects exerted upon a star result in a reduction in its $v_{\text{sin}i}$, a process known as 'magnetic braking' (Kraft, 1967). This is attributable to the magnetised stellar winds carrying angular momentum away from the star (Barnes *et al.*, 2016; See *et al.*, 2024). Skumanich (1972) demonstrates that the surface dynamo area of a star diminishes in conjunction with both $v_{\text{sin}i}$ and time (or age) during the MS phase. Durney (1972) corroborates this hypothesis with the aid of a stellar wind model. Late-type stars (G, K, M) experience magnetic braking from dynamo fields, whereas early-type stars (O, B, A, early-F) exhibit weaker fields due to the presence of less convection. Conversely, the evidence presented by MacGregor & Brenner (1991) indicates that stars may attain a state of 'magnetic saturation' if they rotate at a high rate, which would serve to reduce the loss of angular momentum. Moreover, (D'Antona *et al.*, 2017) put forth a potential explanation for the bimodal rotational distribution observed in binary stars. This explanation postulates that magnetic wind braking or tidal torques exerted by a companion of the binary star could rapidly decelerate $v_{\text{sin}i}$, thereby facilitating a transition from the rapidly rotating track to the non-rotating track (Sun *et al.*, 2020).

The relationship between the distribution of $v_{\text{sin}i}$ and spectral type (ST) has been the subject of investigation since the 1960s (Maeder, 2009). However, these studies have often been limited to specific ST or luminosity class (LC) ranges (Schatzman, 1962; van den Heuvel, 1968; Slettebak & Kusma, 1979; Abt *et al.*, 1997; Royer *et al.*, 2007; Bouvier *et al.*, 2014; AbdulMasih, 2023). In this study, we conduct out using a large sample of stars of various ST observed in different surveys. The objective of this study is to elucidate the relationship between stellar rotation and the ST and LC, which are indirectly related to the effects of the stellar structure and evolution.

The data employed in this study are presented in the following section (Section 2). In Section 3, we provide a methodology for examining the relationship between $v_{\text{sin}i}$ and ST and LC. We discuss the results of this study in Section 4. Finally, the conclusion of this study is summarised in Section 5.

2. Data Set

We select $\sim 50,000$ stars with varying evolutionary statuses from catalogues in the literature that are presented in the Table 1. In order to ensure the reliability of the analysis, we excluded intrinsic variable stars, binary stars and chemically peculiar stars from our study that are mentioned in the catalogues. Following the aforementioned exclusions, the total number of the stars examined in this study is 48,639.

Table 1. The references, the total number of stars and their spectral types (ST) employed in this study are presented in alphabetical order.

References	Total Number of Stars	ST
Chang <i>et al.</i> (2013)	6	A, F
Crossfield (2014)	165	M
Cutispoto <i>et al.</i> (2002)	198	F, G, K
De Medeiros & Mayor (1999)	1540	F, G, K
De Medeiros <i>et al.</i> (2004)	159	F, G, K
De Medeiros <i>et al.</i> (2002a)	134	F, G, K
De Medeiros <i>et al.</i> (2014)	1588	F, G, K
De Medeiros <i>et al.</i> (2002b)	232	F, G, K
Głębocki & Gnacinski (2005)	36,419	O, B, A, F, G, K, M
Holgado <i>et al.</i> (2022)	285	O
Howarth <i>et al.</i> (1997)	185	O, B
Jeffers <i>et al.</i> (2018)	1012	M
López-Valdivia <i>et al.</i> (2019)	221	K, M
Messina <i>et al.</i> (2010)	147	F, G, K, M
Messina <i>et al.</i> (2011)	99	G, K, M
Serebriakova <i>et al.</i> (2023)	145	O, B
Shepard <i>et al.</i> (2020)	9	O
Simón-Díaz & Herrero (2014)	199	O, B
Smith (2015)	48	M
Royer <i>et al.</i> (2002a)	525	B, A, F
Royer <i>et al.</i> (2002b)	2401	B, A, F, G, K
Royer <i>et al.</i> (2007)	1541	B, A, F
Wolff <i>et al.</i> (2004)	143	O, B, A, F, G, K
Wolff <i>et al.</i> (2007)	123	B
Zorec & Royer (2012)	2012	B, A, F

The distribution of the stars in the data set according to STs is presented as a histogram in Figure 1. As is evident from the Figure 1, the majority of the data is concentrated in the F (11536) and G (10454) STs. The data for the B, A and K STs are relatively similar, with numbers of 7670, 9249, and 7072, respectively. The lowest recorded data belongs to stars belonging to the O (961) and M (1232) STs.

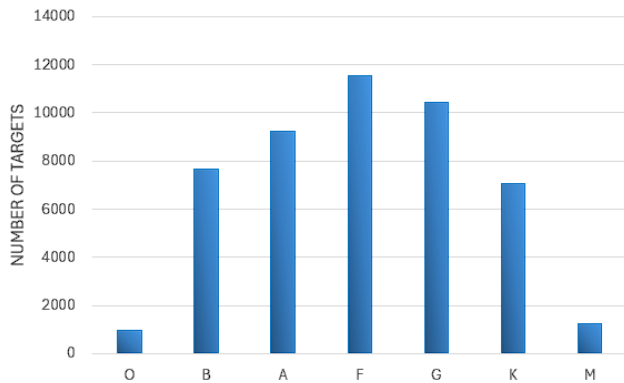


Figure 1. The distribution of stars according to their STs in the data set is presented.

Additionally, the number distribution of LC for the stars is plotted in Figure 2. The data set comprises five distinct LCs: MS (V), subgiant (IV), red giant (III), bright giant (II), and supergiant (I). As plotted in Figure 2, the data set comprises the greatest number of MS stars and the fewest supergiant stars.

The general distribution of the number of stars for each ST is over 200. The number of early-O stars is less than 200, due to the fact that these stars evolve rapidly and are difficult to detect. Similarly, the number of late-K and M stars (as plotted in Figure 2) does not exceed 100. These stars are notoriously challenging to observe due to their low luminosity.

3. Method

A comprehensive methodology was employed to investigate the relationship between STs and $v \sin i$. The analysis commenced with the categorisation of the target stars into two distinct groups based on their STs and LCs. The formation of these groups was undertaken to facilitate investigation into the relationship between $v \sin i$ -STs, as well as the relationship between $v \sin i$ -STs in consideration of LCs.

The rationale for investigating the two subgroups separately is to account for the evolutionary status of the stars and to determine the impact on of this status on stellar rotation.

In order to facilitate the process of coding, each ST is assigned a numerical identifier in the study. Subsequently, the corresponding $v \sin i$ values for each ST were averaged. This enabled an examination of the $v \sin i$ values of the stars over a specified range (Fig. 3). A Gaussian modelling was employed to derive fitting variables for $\langle v \sin i \rangle$ and ST, which were found to follow a normal distribution. In order to achieve the optimal fit, a model consisting of a three-component Gaus-

sian distribution was constructed. The model, based on a Gaussian fit, utilises the amplitude (a), sigma (b) and centre (c) parameters as fitting variables (Eq. 1). In order to constrain the model, full width at half maximum and maximum peak height parameters are also included. The amplitude, sigma and centre parameters represent the strength of the peak, the characteristic width of the peak and centre value of the line to estimate sigma, respectively. The use of constrained parameters, such as full width at half maximum and maximum peak height, allows for the comparison of models. The application of three Gaussian and decaying exponential components in the models facilitates the fitting of multiple peaks and the avoidance of overfitting:

$$g(x) = \sum_{i=1}^3 \frac{a_i}{\sqrt{2\pi b_i^2}} \exp\left(-\frac{(x - c_i)^2}{2b_i^2}\right) + a_i \exp(-x/\tau) \quad (1)$$

This approach eliminates the necessity for parameter boundaries in our models ¹.

4. Results and discussion

4.1 $\langle v \sin i \rangle$ -ST relationship

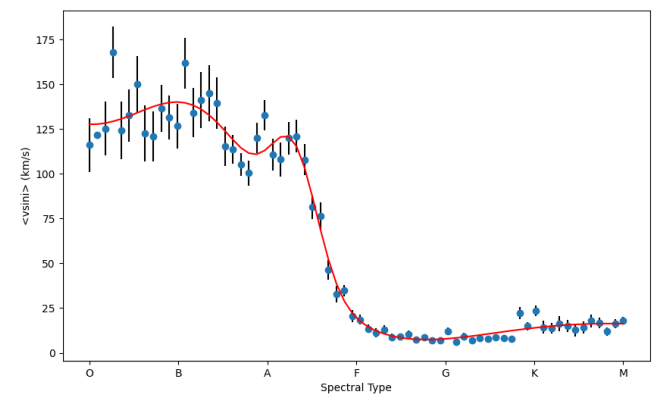


Figure 3. The stellar rotation distribution of the stars in the data set, is represented by a plot of $\langle v \sin i \rangle$ values on the y-axis and STs from O0 to M9 on the x-axis. The red line represents the Gaussian fit.

By employing the Gaussian modelling method, as previously outlined, we have established a general correlation (within the range of O0-M9 range) between ST and $\langle v \sin i \rangle$, as illustrated in Figure 3. Additionally, we

¹A code, designated PYGAUS, has been developed in this study which is capable of averaging and Gaussian modelling of the targets. This code can be applied to Gaussian modelling across a range of ST.

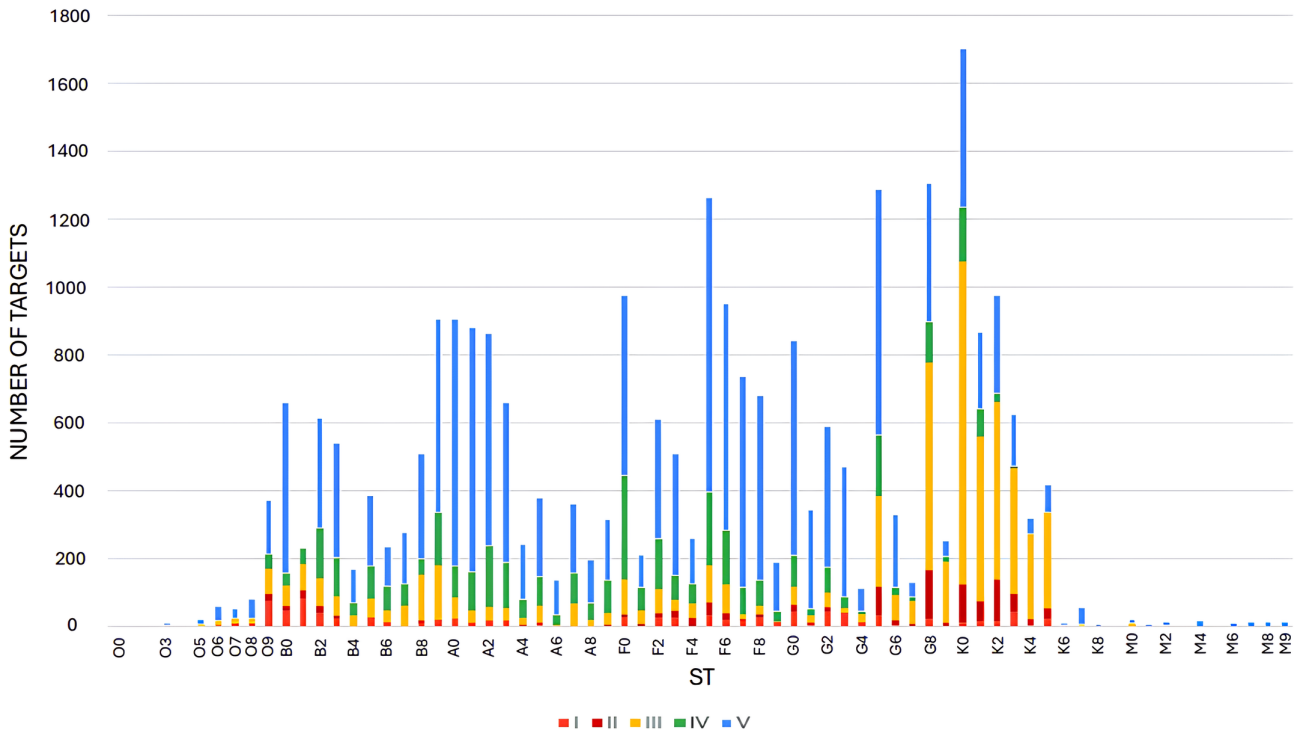


Figure 2. The distribution of stars in the data set according to their detailed STs and LCs. Each ST is divided into subclasses, as indicated by the numbers. In the histogram the colours blue, green, yellow, red and orange represent the MS (V), subgiant (IV), red giant (III), bright giant (II) and supergiant (I), respectively.

have derived relations for the ten distinct STs, taking into account the underlying stellar structure. The resulting fitting parameters for each Gaussian component are presented in Table 2. In addition to Figure 3, comprehensive plots for various ST ranges (O0-F0, F0-M9, O0-F1, F1-M9, O0-F2, F2-M9, O0-F3, F3-M9, O0-F4 and F4-M9), together with their corresponding fits, are presented in Appendix A.

As illustrated in Figure 3, the mean $\langle vsini \rangle$ undergoes an abrupt decline for stars with effective temperatures below the F2 threshold. This phenomenon can be attributed to the displacement of the convective and radiative layers of the stars within the stars, a phenomenon that has been well-documented in the literature. $\langle vsini \rangle$ of late-type stars is significantly reduced as a consequence of the magnetic brake produced by the dynamo process (Kraft, 1967; Rozelot & Neiner, 2009; Ud-Doula *et al.*, 2009).

Skumanich (1972) posits that the mean surface (dynamo) area is proportional to $\langle vsini \rangle$ and decreases in proportion to the inverse square root of time as the star undergoes nuclear fusion on the MS. This remarkable result is demonstrated to be theoretically consistent on the basis of a simple model for the stellar wind proposed by (Durney, 1972). The magnetic fields that cause magnetic braking in late-type stars (G, K and M) are known

to be generated by a dynamo mechanism in which the Coriolis forces associated with stellar rotation deflect convective motions in the recombination regions of H and He (ud-Doula & Owocki, 2002). In contrast, early-type stars (O, B, A, and early-F) with higher initial angular momentum, shorter contraction timescales in the ZAMS, and fully ionised hydrogen in their atmospheres (lacking the strong convection regions associated with hydrogen recombination) are known to exhibit weaker dynamo-induced magnetic fields. This suggests that early-type stars (O, B, A, and early-F) are rotating at a faster rate than late-type stars (late-F, G, K, and M). Nevertheless, as the majority of hot stars typically rotate at high velocity, it is plausible that dynamo production in thin (weak) near-surface convection regions associated with the recombination of fully ionised helium may still occur (ud-Doula & Owocki, 2002). In this regard, we found a significant decrease in $\langle vsini \rangle$ values was observed, amounting to approximately 100 km/s, between hot stars (spectral types O0 to F2) and cool stars (STs F2 to M9).

Figure 3 illustrates the high rotational velocities of O-type stars, which have been the subject of a recent study by Britavskiy *et al.* (2023). This study examined and discussed the potential relationship between these rapid rotation rates and binary star systems. The find-

Table 2. The amplitude (a), sigma (b), and centre (c) parameters of the Gaussian components obtained from the i th Gaussian fit for the different ranges of ST are presented. To achieve the optimal fit, a model consisting of three Gaussians was constructed. The value of i represents the number of Gaussians used.

	i	a	b	c
O0-M9	1	104.15	9.47	16.39
	2	59.17	2.91	28.70
	3	15.60	10.21	65.09
O0-F0	1	114.54	3.62	15.90
	2	118.63	6.31	27.42
	3	135.18	4.10	6.58
F0-M9	1	9.30	12.69	31.73
	2	812.32	7.38	14.97
	3	16.29	9.92	65.06
O0-F1	1	116.89	4.43	27.61
	2	132.30	4.20	16.53
	3	135.77	4.51	5.86
F1-M9	1	47.03	0.04	61.37
	2	8.95	6.80	64.40
	3	338.71	5.44	22.01
O0-F2	1	134.27	4.08	16.18
	2	117.72	4.74	27.47
	3	127.23	3.88	6.48
F2-M9	1	11.44	7.33	35.61
	2	16.64	10.35	64.32
	3	40.00	2.90	31.33
O0-F3	1	140.93	4.75	16.22
	2	113.96	4.14	27.87
	3	110.18	3.50	6.29
F3-M9	1	16.60	9.87	64.53
	2	9.73	8.84	35.20
	3	33.91	3.29	31.39
O0-F4	1	134.39	4.32	16.72
	2	116.80	4.13	27.72
	3	135.22	4.55	5.85
F4-M9	1	153.23	4.91	25.58
	2	5.16	5.37	75.96
	3	10.05	7.68	63.74

ings revealed that a significant portion of the rapidly rotating O-type star population is associated with binary interactions.

The fastest stars in Figure 3, as determined by their peak shapes, are of the B- and A-type stars. Among them, the early-A stars, which manifest as a distinct peak in Figure 3, are the fastest stars. It has been observed that there is a notable decline in the velocity of late-A stars, with a reduction of approximately 40 km/s, as they transition towards early-F stars.

In contrast to the convective envelopes observed in

the late-A type stars, those of early-A type stars are notably absent (Abt & Morrell, 1995; Royer *et al.*, 2007). Late-A type stars are situated in close proximity to the boundary at which the convective envelope becomes apparent in the stellar photosphere, as illustrated in the Hertzsprung-Russell diagram (HRD). It has been observed that late-A type stars are situated in close proximity to the granulation boundary, a phenomenon that is exclusive to MS stars. In the case of evolved late-A type stars, their position in the HRD is found to be significantly bluer than the granulation boundary. A detailed discussion of this situation can be found in Section 4.2. An additional factor contributing to this phenomenon is that examining stellar rotation as a mean can be somewhat deceptive. This is due to the fact that early-A type stars exhibit both high and low stellar rotation velocities, which are consistent with observations presented by Abt & Morrell (1995). They identified a bimodal distribution of stellar rotational velocities among A-type MS stars.

A comparable phenomenon is observed in M-type stars, albeit with a considerably diminished rate of change in the $\langle v \sin i \rangle$, estimated at ~ 20 km/s. As illustrated in Figure 3, early-M stars can be identified as a peak. Delfosse *et al.* (1998) and Mohanty & Basri (2003) posit that saturation-type rotation-activity is observed in M5- to M8.5-type stars, resulting in an increase of approximately 5-10 km/s in the $v \sin i$ of these stars. As illustrated in Figure 3, the $v \sin i$ of M9-type stars exhibits a notable decline due to a precipitous decline in activity (Deshpande *et al.*, 2013). Moreover, metal-poor M-type stars are observed to be more compact and exhibit higher rotational velocities for a given mass (Mohanty & Basri, 2003). These effects may provide an explanation for the slight increase in stellar rotation velocity observed in M-type stars. Figure 3 illustrates that late-M stars exhibit a markedly higher $\langle v \sin i \rangle$ than their early-M counterparts. This may be attributed to the two dynamo processes that are strongly coupled to the rotation in stars composed entirely of the convective layer (Fan, 2021). It is important to note that the studies mentioned above only concern M dwarfs, whereas our study also encompasses evolved M-type stars. We demonstrated that the overall $v \sin i$ -ST distribution of our data, as represented by the Gaussian-fitted line in Figure 5 of the Appendix, is consistent with the aforementioned findings.

4.2 $\langle v \sin i \rangle$ -LC relationship

As previously stated in Section 2, our data set also encompasses stars that are at disparate evolutionary stages. Accordingly, the LCs were divided into five subgroups: supergiants, bright giants, red giants, subgiants and MS stars. To elucidate the correlation be-

Table 3. The same methodology as that employed in Table 2 is used here, but the LCs are divided into five subgroups, as follows: supergiants, bright giants, red giants, subgiants and MS stars.

	i	a	b	c
Supergiant	1	140.39	5.60	3.67
	2	42.54	16.97	9.30
	3	10.72	36.58	14.08
Bright Gaint	1	95.01	9.53	4.08
	2	46.21	26.59	9.85
	3	161.31	79.47	2.79
Red Giant	1	140.20	122.01	27.97
	2	72.55	28.69	6.62
	3	108.16	9.34	7.75
Subgiant	1	109.28	15.38	6.19
	2	95.99	28.80	4.04
	3	11.82	55.37	17.17
MS	1	148.05	12.36	12.27
	2	66.36	28.21	3.35
	3	10.41	69.36	13.24

tween LC and $\langle vsini \rangle$, the methodology employed for ST was replicated. The derived parameters for each LC are presented in Table 3. Figure 4 illustrates the distribution of $\langle vsini \rangle$ with ST for single stars at disparate evolutionary stages.

It is a well-established fact that as stars evolve, their $vsini$ tends to decrease (Herbig & Spalding, 1953, 1955; Kraft & Wilson, 1965; Gray & Nagar, 1985; Gray & Toner, 1986, 1987). Figure 4 illustrates the decline in $vsini$ that occurs during the later stages of the stellar evolution for each ST. As the star exhausts its hydrogen in its core, radiation pressure cannot resist the force of gravity. As a result, the core undergoes a reduction in size, yet the expansion of the hydrogen-burning shell within the envelope results in the the opposite effect. This leads to an increase in the moment of inertia (Weber & Davis, 1967). Consequently, as the star evolves towards the giant branch, the moment of inertia increases, which results in a decrease in stellar rotation (de Medeiros *et al.*, 1996; Krishnamurthi *et al.*, 1997). Given the increase in stellar radius that occurs during the later stages of MS evolution, a decrease in $vsini$ is to be expected. Moreover, mass loss during the subsequent evolutionary stages of the star also contributes to this decrease. In the case of cool stars, the dynamo process and magnetic braking represent additional factors that contribute to the slowdown of $vsini$ (Gray, 1981, 1982, 1983). In contrast, for hot stars, an additional contribution to the slowdown is provided by stellar winds (de Freitas *et al.*, 2022). A decrease in $vsini$ is also observed in the MS for A-type

evolved stars. However, as stars evolve, the granulation boundary shifts to the hotter region in Figure 4, and the change is manifested in the hotter region in accordance with the stages of evolution. This situation is most obvious in the evolutionary stages after the subgiant evolutionary stage.

5. Conclusion

The STs of stars provide insight into their internal structure. The stellar structure is influenced by various parameters, including $vsini$. In this study, we analysed the relation between $vsini$ and ST using data on approximately 50,000 non-variable and single stars at different evolutionary stages and with a broad range range of STs from O0 to M9. Our findings revealed $\langle vsini \rangle$ distributions of early- and late-type stars.

In many contemporary studies, P_{rot} is commonly used instead of direct measurements of stellar rotational velocities. However, in our dataset comprising 50,000 stars, our objective was to demonstrate variations in stellar rotation across STs in a more transparent manner by utilising $vsini$. By focusing solely on single stars, we also sought to maintain the reliability of our analysis, with the expectation that this approach would enable more precise estimations of stellar velocities. Moreover, our findings revealed a shift in the correlation between ST and $\langle vsini \rangle$ as stars evolve.

In subsequent studies, the investigation will be expanded to encompass chemically peculiar stars and cluster member stars, with the objective of acquiring a more profound comprehension of the underlying mechanisms that regulate the influence of stellar abundance on stellar rotation.

Acknowledgements

In conducting this study, the bibliographic service NASA Astrophysics Data System, SIMBAD and VizieR online catalogue were employed. This study was supported by the Scientific and Technological Research Council of Turkey (TÜBİTAK) under Grant Number 2209A-1919B012310850. The authors thank TÜBİTAK for their support.

We would like to express our gratitude to İbrahim Küçük and Nur Filiz Ak for their valuable comments and insightful discussions on the manuscript. Furthermore, we are indebted to Maria Granados Serrano and Sertaç Bera Yurtaslan for their assistance in reviewing and refining the language of the revised manuscript.

The PYGAUS code, which is capable of performing averaging and Gaussian modelling of the tar-

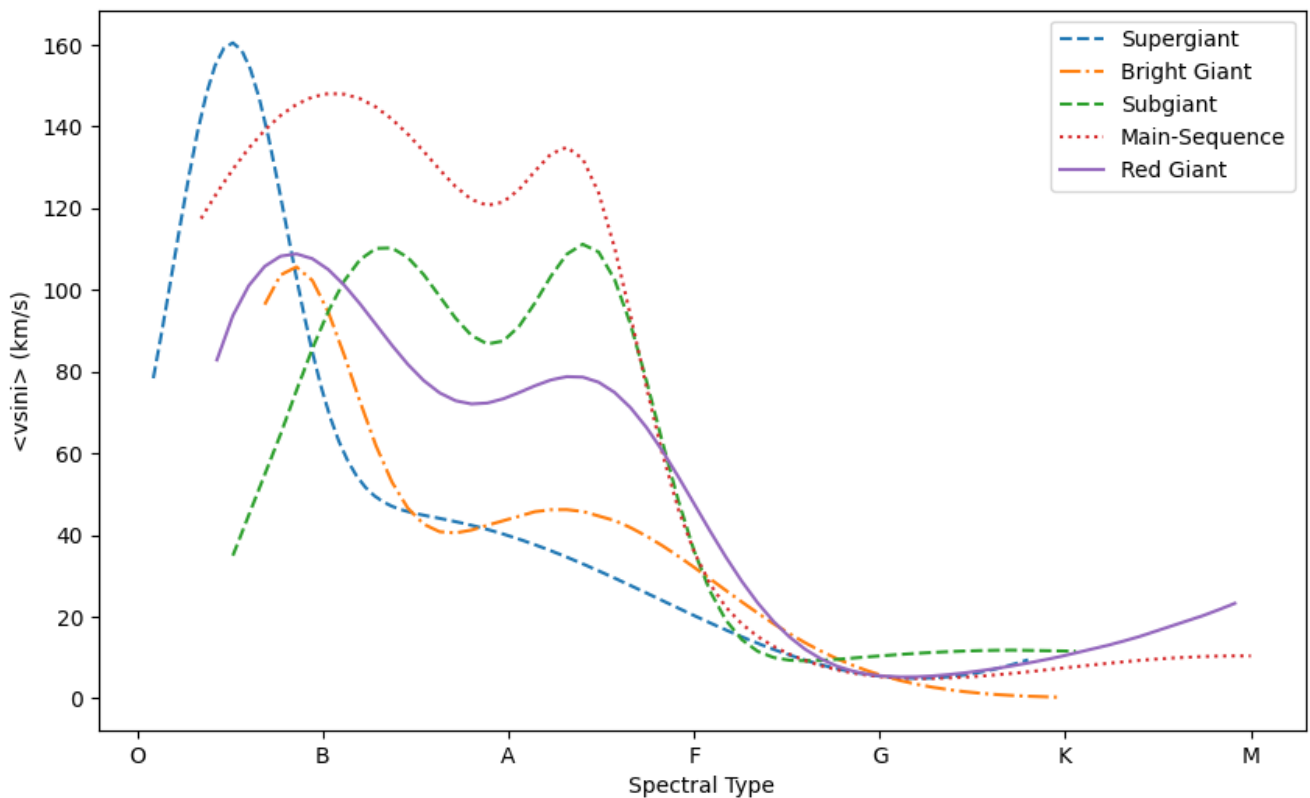


Figure 4. The distribution of $\langle vsini \rangle$ versus ST for single stars of varying evolutionary statuses. The x-axis and y-axis represent the STs from O0 to M9 and the $\langle vsini \rangle$ values, respectively. The Gaussian-fitted lines for supergiant, bright giant, red giant, subgiant and MS are represented by blue, orange, purple, green and red colours, respectively.

gets, can be accessed at the following the URL: <https://github.com/MertBoranSt/PYGAUS>.

References

- Abdul-Masih, M. 2023, *A&A*, 669, L11
- Abt, H. A., & Morrell, N. I. 1995, *APJS*, 99, 135
- Abt, H. A., Tan, H., & Zhou, H. 1997, *ApJ*, 487, 365
- Armitage, P. J., & Clarke, C. J. 1996, *MNRAS*, 280, 458
- Barnes, S., Sofia, S., & Pinsonneault, M. 2001, *ApJ*, 548, 1071
- Barnes, S. A., Weingrill, J., Fritzewski, D., Strassmeier, K. G., & Platais, I. 2016, *APJ*, 823, 16
- Bouvier, J., Matt, S. P., Mohanty, S., *et al.* 2014, in *Protostars and Planets VI*, ed. H. Beuther, R. S. Klessen, C. P. Dullemond, & T. Henning, 433–450
- Britavskiy, N., Simón-Díaz, S., Holgado, G., *et al.* 2023, *aa*, 672, A22
- Chang, S. W., Protopapas, P., Kim, D. W., & Byun, Y. I. 2013, *AJ*, 145, 132
- Che, X., Monnier, J. D., Zhao, M., *et al.* 2011, *ApJ*, 732, 68
- Cieza, L., & Baliber, N. 2007, *ApJ*, 671, 605
- Collier Cameron, A., & Campbell, C. G. 1993, *AaA*, 274, 309
- Costa, G., Girardi, L., Bressan, A., *et al.* 2019, *MNRAS*, 485, 4641
- Crossfield, I. J. M. 2014, *A&A*, 566, A130
- Cutispoto, G., Pastori, L., Pasquini, L., *et al.* 2002, *A&A*, 384, 491
- D’Antona, F., Milone, A. P., Tailo, M., *et al.* 2017, *Nature Astronomy*, 1, 0186
- de Freitas, D. B., Cavalcante, F. J., & Santiago, T. M. 2022, *EPL (Europhysics Letters)*, 140, 29001
- De Medeiros, J. R., Alves, S., Udry, S., *et al.* 2014, *A&A*, 561, A126

- de Medeiros, J. R., Da Rocha, C., & Mayor, M. 1996, *AAP*, 314, 499
- De Medeiros, J. R., Da Silva, J. R. P., & Maia, M. R. G. 2002a, *ApJ*, 578, 943
- De Medeiros, J. R., & Mayor, M. 1999, *A&AS*, 139, 433
- De Medeiros, J. R., Udry, S., Burki, G., & Mayor, M. 2002b, *A&A*, 395, 97
- De Medeiros, J. R., Udry, S., & Mayor, M. 2004, *A&A*, 427, 313
- Delfosse, X., Forveille, T., Perrier, C., & Mayor, M. 1998, *AAA*, 331, 581
- Deshpande, R., Blake, C. H., Bender, C. F., *et al.* 2013, *AJ*, 146, 156
- Durney, B. 1972, *ApSS*, 17, 489
- Fan, Y. 2021, *Living Reviews in Solar Physics*, 18, 5
- Gallet, F., & Bouvier, J. 2013, *A&A*, 556, A36
- Głębocki, R., & Gnaciński, P. 2005, in *ESA Special Publication, Vol. 560, 13th Cambridge Workshop on Cool Stars, Stellar Systems and the Sun*, ed. F. Favata, G. A. J. Hussain, & B. Battrick, 571
- Gray, D. F. 1981, *APJ*, 251, 155
- . 1982, *JRASC*, 76, 319
- Gray, D. F. 1983, in *Solar and Stellar Magnetic Fields: Origins and Coronal Effects*, ed. J. O. Stenflo, Vol. 102, 461–465
- Gray, D. F., & Nagar, P. 1985, *APJ*, 298, 756
- Gray, D. F., & Toner, C. G. 1986, *APJ*, 310, 277
- . 1987, *ApJ*, 322, 360
- Harris, C. R., Millman, K. J., van der Walt, S. J., *et al.* 2020, *Nature*, 585, 357
- Herbig, G. H., & Spalding, J. F., J. 1953, *PAPS*, 65, 192
- Herbig, G. H., & Spalding, John F., J. 1955, *APJ*, 121, 118
- Holgado, G., Simón-Díaz, S., Herrero, A., & Barbá, R. H. 2022, *A&A*, 665, A150
- Howarth, I. D., Siebert, K. W., Hussain, G. A. J., & Prinja, R. K. 1997, *MNRAS*, 284, 265
- Hunter, J. D. 2007, *Computing in Science & Engineering*, 9, 90
- Jeffers, S. V., Schöfer, P., Lamert, A., *et al.* 2018, *A&A*, 614, A76
- Jermyn, A. S., Tout, C. A., & Chitre, S. M. 2018, *MNRAS*, 480, 5427
- Koenigl, A. 1991, *ApJl*, 370, L39
- Kraft, R. P. 1967, *ApJ*, 150, 551
- Kraft, R. P., & Wilson, O. C. 1965, *APJ*, 141, 828
- Krishnamurthi, A., Pinsonneault, M. H., Barnes, S., & Sofia, S. 1997, *APJ*, 480, 303
- López-Valdivia, R., Mace, G. N., Sokal, K. R., *et al.* 2019, *ApJ*, 879, 105
- MacGregor, K. B., & Brenner, M. 1991, *ApJ*, 376, 204
- Maeder, A. 2009, *Physics, Formation and Evolution of Rotating Stars* (Springer Berlin Heidelberg), doi:10.1007/978-3-540-76949-1
- McAlister, H. A., ten Brummelaar, T. A., Gies, D. R., *et al.* 2005, *ApJ*, 628, 439
- Messina, S., Desidera, S., Lanzafame, A. C., Turatto, M., & Guinan, E. F. 2011, *A&A*, 532, A10
- Messina, S., Desidera, S., Turatto, M., Lanzafame, A. C., & Guinan, E. F. 2010, *A&A*, 520, A15
- Meynet, G., & Maeder, A. 2000, *A&A*, 361, 101
- Mohanty, S., & Basri, G. 2003, in *Cambridge Workshop on Cool Stars, Stellar Systems, and the Sun, Vol. 12, The Future of Cool-Star Astrophysics: 12th Cambridge Workshop on Cool Stars, Stellar Systems, and the Sun*, ed. A. Brown, G. M. Harper, & T. R. Ayres, 683–688
- Newville, M., Stensitzki, T., Allen, D. B., & Ingargiola, A. 2015, in *LMFIT: Non-Linear Least-Square Minimization and Curve-Fitting for Python* (Zenodo)
- Rebull, L. M., Stauffer, J. R., Megeath, S. T., Hora, J. L., & Hartmann, L. 2006, *ApJ*, 646, 297
- Royer, F., Gerbaldi, M., Faraggiana, R., & Gómez, A. E. 2002a, *A&A*, 381, 105
- Royer, F., Grenier, S., Baylac, M. O., Gómez, A. E., & Zorec, J. 2002b, *A&A*, 393, 897
- Royer, F., Zorec, J., & Gómez, A. E. 2007, *A&A*, 463, 671

- Rozelot, J.-P., & Neiner, C. 2009, The Rotation of Sun and Stars, 1st edn., Lecture Notes in Physics (Springer Berlin, Heidelberg), X, 264, copyright Springer-Verlag Berlin Heidelberg 2009, doi:10.1007/978-3-540-87831-5
- Schatzman, E. 1962, *Annales d’Astrophysique*, 25, 18
- See, V., Lu, Y. L., Amard, L., & Roquette, J. 2024, *MNRAS*, 533, 1290
- Serebriakova, N., Tkachenko, A., Gebruers, S., *et al.* 2023, *A&A*, 676, A85
- Shepard, K., Gies, D. R., Lester, K. V., *et al.* 2020, *ApJ*, 888, 82
- Simón-Díaz, S., & Herrero, A. 2014, *A&A*, 562, A135
- Skumanich, A. 1972, *ApJ*, 171, 565
- Slettebak, A., & Kusma, T. J. 1979, in *IAU Colloq. 47: Spectral Classification of the Future*, Vol. 9, 87
- Smith, C. L. 2015, PhD thesis, Georgia State University
- Sun, W., Li, C., Deng, L., & de Grijs, R. 2020, in *IAU Symposium*, Vol. 351, *Star Clusters: From the Milky Way to the Early Universe*, ed. A. Bragaglia, M. Davies, A. Sills, & E. Vesperini, 228–232
- ud-Doula, A., & Owocki, S. P. 2002, *ApJ*, 576, 413
- Ud-Doula, A., Owocki, S. P., & Townsend, R. H. D. 2009, *MNRAS*, 392, 1022
- van den Heuvel, E. P. J. 1968, *Bull. Astron. Inst.*, 19, 309
- von Zeipel, H. 1924, *MNRAS*, 84, 665
- Weber, E. J., & Davis, Leverett, J. 1967, *APJ*, 148, 217
- Wolff, S. C., Strom, S. E., Dror, D., & Venn, K. 2007, *AJ*, 133, 1092
- Wolff, S. C., Strom, S. E., & Hillenbrand, L. A. 2004, *ApJ*, 601, 979
- Zorec, J., & Royer, F. 2012, *A&A*, 537, A120
- matplotlib (Hunter, 2007), numpy (Harris *et al.*, 2020), pandas² and lmfit (Newville *et al.*, 2015).

Appendix A. The overall *vsini*-ST distribution of the data set

Appendix B. PYGAUS code

The PYGAUS code is utilised to ensure the efficient and consistent application of a Gaussian model to the pertinent data. The code incorporates Python libraries:

²<https://pandas.pydata.org/>

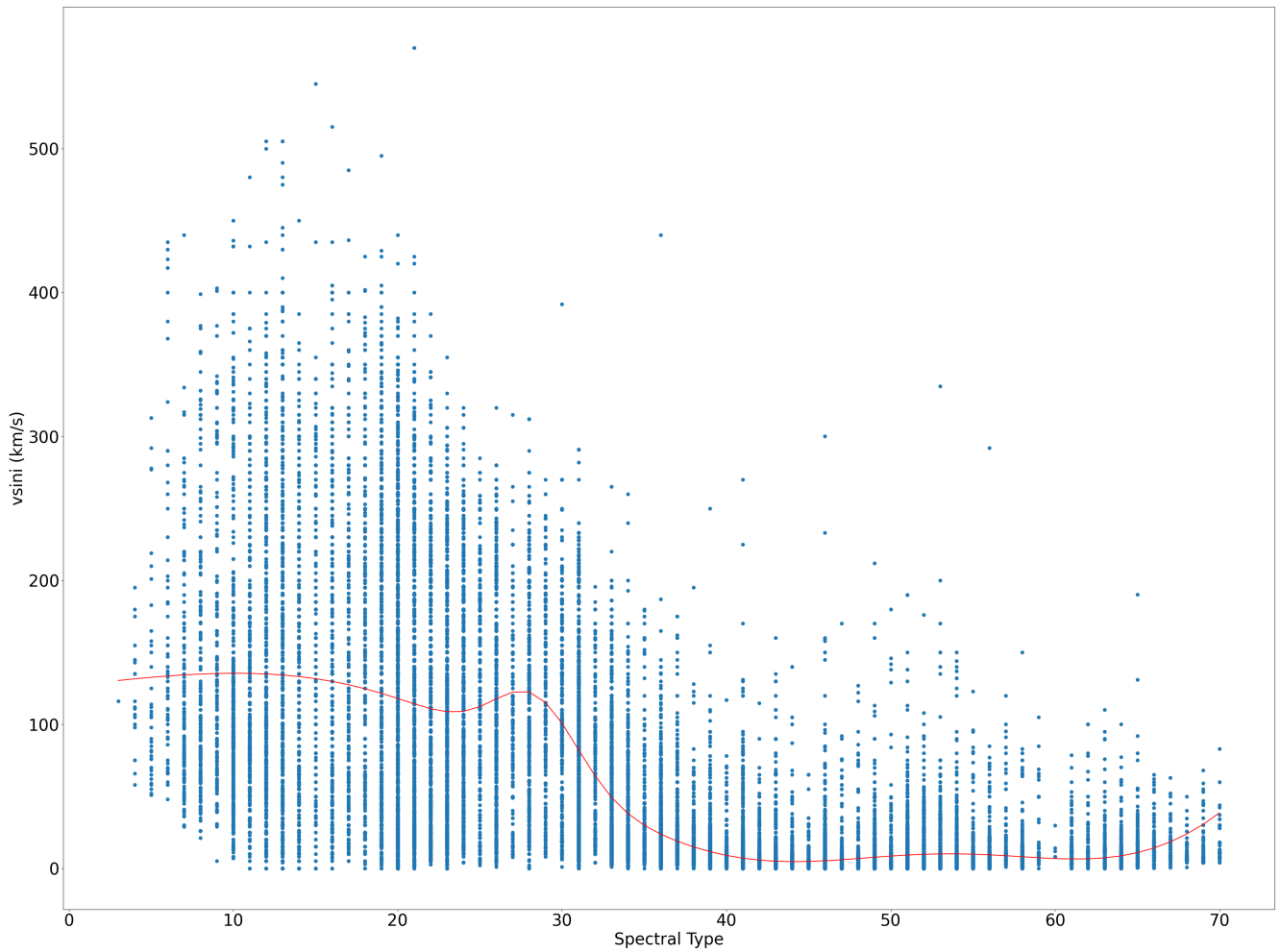


Figure 5. The overall $v \sin i$ -ST distribution of the data set. The x-axis and y-axis represent the STs, ranging from O0 to M9, and the $v \sin i$ values, respectively. The red line represents the Gaussian fit to all stars which are investigated in this study.